Characterization of submicron organic particles in Beijing during summertime: Comparison between SP-AMS and HR-AMS

Junfeng Wang[1,2], Jianhuai Ye[2], Dantong Liu[3], Yangzhou Wu[3], Jian Zhao[4], Weiqi Xu[4], Conghui Xie[4], Fuzhen Shen[1], Jie Zhang[5], Paul E. Ohno[2], Yiming Qin[2], Xiuyong Zhao[6], Scot T. Martin[2], Alex K.Y. Lee[7], Pingqing Fu[8], Daniel J. Jacob[2], Qi Zhang[9], Yele Sun[4], Mindong Chen[1] and Xinlei Ge[1,*]

[1]Jiangsu Key Laboratory of Atmospheric Environment Monitoring and Pollution Control, Collaborative Innovation Center of Atmospheric Environment and Equipment Technology, School of Environmental Science and Engineering, Nanjing University of Information Science and Technology, Nanjing, China

[2]School of Engineering and Applied Sciences, Harvard University, Cambridge, MA, United States

[3]Department of Atmospheric Sciences, School of Earth Sciences, Zhejiang University, Hangzhou, China

[4]State Key Laboratory of Atmospheric Boundary Layer Physics and Atmospheric Chemistry, Institute of Atmospheric Physics, Chinese Academy of Sciences, Beijing, China

[5]Department of Atmospheric Science, Colorado State University, Fort Collins, CO, United States

[6]State Environmental Protection Key Laboratory of Atmospheric Physical Modeling and Pollution Control, State Power Environmental Protection Research Institute, Nanjing, China

[7]Department of Civil and Environmental Engineering, National University of Singapore, Singapore

[8]Institute of Surface-Earth System Science, Tianjin University, Tianjin, China

[9]Department of Environmental Toxicology, University of California Davis, Davis, CA, United States

*Corresponding author: Xinlei Ge (Email: caxinra@163.com)

1 **ABSTRACT**

2   Black carbon (BC) particles in Beijing summer haze play an important role in

3 regional radiation balance and related environmental processes. Understanding the

4 factors that lead to variability of the impacts of BC remains limited. Here, we present

5 observations by a soot-particle aerosol mass spectrometer of BC-containing submicron

6 particulate matter (BC-PM_1) in Beijing, China during 2017 summer. These observations

7 were compared to concurrently measured total non-refractory submicron particulate

8 matter (NR-PM_1) by a high-resolution aerosol mass spectrometer (HR-AMS). Distinct

9 properties were observed between NR-PM_1 and BC-PM_1 relevant to organic aerosol

10 (OA) composition. Hydrocarbon-like OA in BC-PM_1 was found to be up to two-fold

11 higher than that in NR-PM_1 in fresh vehicle emissions, suggesting that a part of HOA

12 in BC-PM_1 may be overestimated, likely due to the change of collection efficiency of

13 SP-AMS. Cooking-related OA was only identified in NR-PM_1, whereas aged biomass

14 burning OA (A-BBOA) was a unique factor only identified in BC-PM_1. The A-BBOA

15 was linked to those heavily coated BC, which may lead to enhancement of light

16 absorption ability of BC by a factor of two via the "lensing effect". More-oxidized

17 oxygenated OA identified in BC-containing particles was found to be slightly different

18 from that observed by HR-AMS, mainly due to the influence of A-BBOA. Overall,

19 these findings highlight that BC in urban Beijing is partially of agricultural fire origin

20 and, a unique biomass burning-related OA associated with BC may be ubiquitous in

21 aged BC-PM_1, and this OA may play a role in affecting air quality and climate that has

22 not previously been fully considered.

1. Introduction

Black carbon (BC) is an important component of atmospheric aerosol that exerts negative effects on regional radiation balance (Bond et al., 2013) and human health (Janssen, 2012). It absorbs solar radiation, leading to direct atmospheric heating (Ramanathan and Carmichael, 2008). Indirectly, BC-containing particles (BCc) can also serve as cloud condensation nuclei upon mixing with hydrophilic species (e.g., sulfate), resulting in changes in cloud properties (Wu et al., 2019). Inhalation of BC is associated with adverse health impacts such as respiratory diseases and birth defects (Janssen, 2012).

BC particles are released to the atmosphere directly and usually mixed with non-BC materials (e.g., inorganic and organic) from incomplete fuel combustion and open fires (Ramanathan and Carmichael, 2008;Bond et al., 2013;Chen et al., 2013). Non-BC species also can coat onto primary BCc in the atmosphere through condensation and/or coagulation processes (Lee et al., 2017). These atmospheric processes gradually alter the mixing state and the morphology (e.g., from an externally-mixed fractal structure (Buseck et al., 2014) into an internally-mixed "core-shell" structure (China et al., 2015)) of BCc. These alterations can enhance the light absorption capacity of the BC core via the "lensing effect" due to the increased light absorption cross-section as a result of the enhanced coating thickness (Saleh et al., 2015;Cappa et al., 2012). Additionally, the chemical constituents of BCc may dynamically change during the aging processes, which also lead to changes in the light absorption capacity of the particles (Wang et al., 2019;Wang et al., 2017). Because these physical and chemical processes of both organic and inorganic species inside BCc continuously alter particle properties throughout the lifetime of the particles, great uncertainty remains in quantifying the light absorption ability of BC (Liu et al., 2018;Liu et al., 2019). Understanding the relationship of mixing state and chemical composition to the light absorption properties of BCc, as well as its spatiotemporal distribution, is of importance to accurately evaluate the impacts of BC in regional air quality.

Aerodyne high-resolution aerosol mass spectrometry (HR-AMS) (Canagaratna et al., 2007) has been widely applied in field studies to investigate the chemically-resolved

composition of non-refractory submicron particulate matter (NR-PM$_1$, species that vaporize at temperature < 600 °C)(Li et al., 2015;Lee et al., 2013;Sun et al., 2012;Ge et al., 2012b;Ge et al., 2012a;Xu et al., 2019b;Sun et al., 2014). However, the working temperature of the standard HR-AMS tungsten vaporizer (600 ºC) is not sufficient to vaporize refractory species such as BC. To overcome this limitation, soot-particle aerosol mass spectrometry (SP-AMS) is developed (Onasch et al., 2012). In addition to the standard tungsten vaporizer, SP-AMS is equipped with a laser vaporizer (with a wavelength of 1064 nm) which selectively heats BC (core), together with the non-BC species mixed with it (Wang et al., 2016). This novel technique makes it possible to compare the compositions of submicron BCc (BC-PM$_1$) and NR-PM$_1$, allowing a more accurate assessment of the impacts of BC. However, a question is whether the ion fragments of organic species ionized by the 70eV electron impact of SP-AMS and HR-AMS are the same in terms of different thermal schemes. It has been reported that the mass spectra of NR-PM$_1$ organic have high m/z 44 (mainly CO_2^+) signal, while the mass spectra of BC-related organics have high m/z 43 ($C_3H_7^+$ and $C_2H_3O^+$) signal. The reason for this is the SP-AMS provides vaporization of the BC-PM$_1$ at lower temperatures compared to the standard tungsten vaporizer of the HR-AMS, resulting in less overall fragmentation and therefore less CO_2^+ production in the laser, in addition, the lower fragmentation also causes the presence of more ion fragments at m/z > 100 amu in the SP-AMS mass spectra compared to that of HR-AMS (Canagaratna et al., 2015b;Massoli et al., 2015). Nevertheless, quantification of BC-PM$_1$ organic aerosol (OA) factors identified from positive matrix factorization (PMF) has been reported that were not significantly affected by the differences of mass spectra between HR-AMS and SP-AMS (Lee et al., 2017;Massoli et al., 2015).

To date, there have only been a few studies that have compared the differences of species in BC-PM$_1$ and NR-PM$_1$ (Lee et al., 2017;Collier et al., 2015;Massoli et al., 2015). Lee et al. found that cooking-related organic aerosol (COA) may externally mix with BC in summertime California (Lee et al., 2017). The COA factor was identified in NR-PM$_1$ organic aerosol (OA), but not in the BC-related OA. Wang et al found that transported biomass burning organic aerosol could be thickly coated on BC in central

83 Tibetan Plateau and significantly enhance the light absorption capacity of BC cores

84 (Wang et al., 2017). Interestingly, the transported biomass burning organic aerosol was

85 not resolved in NR-PM$_1$ OA particles from concurrent HR-AMS measurements (Xu et

86 al., 2018). These studies suggest that BC-related OA may undergo different

87 atmospheric processes compared to those do not contain BC.

88   Beijing is a megacity known for high particulate matter (PM) concentrations. BC-

89 PM$_1$ during haze events of summertime Beijing may have distinct sources and

90 properties than other locations in the world. As a part of the UK-China Air Pollution

91 and Human Health (APHH) project summer campaign (Shi et al., 2019; Chen et al.,

92 2020a; Chen et al., 2020b), in this study, we focus on the differences of individual

93 species between BC-PM$_1$ and NR-PM$_1$ regarding their chemical composition, mass

94 loadings, sources, and formation pathways in summertime in urban Beijing. Results

95 from this study provide a better understanding of the formation mechanism of OA

96 particles in Beijing haze and valuable insights in assessing their impacts on air quality.

97

98 **2. Experiments**

99 **2.1. Sampling site and period**

100   The observations were conducted at a rooftop laboratory (8 m above ground level)

101 in the Tower Division of the Institute of Atmospheric Physics (IAP), Chinese Academy

102 of Sciences (CAS) in urban Beijing (39º58′N, 116º22′E), China, from 4 to 29 June,

103 2017. This site has been reported multiple times to be a typical urban observation

104 location (Xie et al., 2019b;Liu et al., 2019;Wang et al., 2019;Qiu et al., 2019;Xu et al.,

105 2019a;Xie et al., 2019a). The site is located around the North 3rd Ring Road of Beijing.

106 A highway is approximately 360 m to the east and a lot of restaurants (e.g., Sichuan

107 style and BBQ) are within 100 m on the north side.

108

109 **2.2. Instrumentation**

110   Two Aerodyne Aerosol Mass Spectrometers (AMS), including a laser-only Soot-

111 Particle AMS (SP-AMS) and a High-Resolution Time of Flight AMS (HR-AMS) were

112 deployed to measure chemical compositions and size distributions of BC-PM$_1$ and NR-

113 PM$_1$, respectively. Three types of species were measured during the campaign: NR-
114 PM$_1$, including non-refractory species that don't mix with BC (Type I) and non-
115 refractory species that mixed with BC (Type II), and BC-PM$_1$ (BC core and both
116 refractory and non-refractory species coated on the core)(Type III). NR-PM$_1$ can be
117 quickly vaporized by the 600 ºC tungsten vaporizer of HR-AMS and be detected. The
118 SP-AMS used here was equipped only with the Nd-YAG intra-cavity infrared laser
119 (1064 nm) (tungsten vaporizer was physically removed), it can selectively detect BC-
120 containing particles only, which include Type II and Type III species. A shared PM$_{2.5}$
121 cyclone inlet (Model URG-2000-30ED) with 3 Lpm flowrate and a diffusion dryer were
122 used prior to the sampling. The detailed information on the operation of HR-AMS and
123 SP-AMS during the sampling campaign can be found in previous literature (Xie et al.,
124 2019a;Xu et al., 2019b). Details of tuning, calibration, and configurations of the two
125 AMS instruments can be seen in our previous papers (Wang et al., 2019;Xu et al.,
126 2019a;Xu et al., 2019b). The two AMS were operated under the V-mode which is
127 favorable for mass quantification with a time resolution of five minutes. Mixing ratios
128 of O$_3$, and NO$_2$ (Thermo Fisher Scientific, model 49i and model 42C) were measured
129 in parallel simultaneously. Vertical meteorological parameters, including temperature
130 (*T*) and relative humidity (*RH*), were measured from the IAP 325m meteorological
131 tower.

132

133 **2.3. Data Analysis**

134   AMS data analysis was performed by using Squirrel 1.57 and Pika 1.16I based on
135 Igor Pro 6.37 (WaveMetrics Corp.). The measurement of filtered air was performed for
136 24 hours before the start of the campaign to determine the detection limits of various
137 aerosol species and to adjust the fragmentation table. The relative ionization efficiency
138 (RIE) of BC was calibrated with Regal Black (RB, REGAL 400R pigment black, Cabot
139 Corp.). The average ratio of C$_1^+$ to C$_3^+$ ionized from pure BC (RB) was determined to
140 be 0.53, which minimizes the influence of C$_1^+$ from non-refractory organics. The RIE
141 of BC was determined to be 0.17 based on calibrations performed before, in the middle,
142 and at the end of the campaign. RIEs of NO$_3^-$, SO$_4^{2-}$, NH$_4^+$ were determined to be 1.1,

143   0.82, and 3.82, respectively, and default values of 1.3 and 1.4 for RIEs of Chl and Org

144   were applied, respectively (Canagaratna et al., 2007). Consistent with BC-PM$_1$

145   measurements in previous studies, the RIEs calibration of NO_3^-, SO_4^{2-}, NH_4^+ were

146   performed before the tungsten vaporizer was removed, by assuming those RIEs remain

147   unchanged throughout the campaign (Wang et al., 2017). Polystyrene latex (PSL)

148   spheres (100-700 nm) (Duke Scientific Corp., Palo Alto, CA) were used to calibrate the

149   particle size distribution before the campaign. The collection efficiency (CE) of 0.5

150   were applied for both HR-AMS and SP-AMS in this study. It should be noted that, the

151   BC quantification will not be affected by particle bouncing without the tungsten

152   vaporizer, which could affect the CE in the standard HR-AMS measurements

153   (Canagaratna et al., 2007). However, the CE will be governed by the overlap of particle

154   beam and laser beam (Lee et al., 2017;Massoli et al., 2015;Willis et al., 2014). Both

155   HR-AMS and SP-AMS resolved mass concentrations of NR-PM$_1$ and BC were

156   calculated based on V-mode high-resolution fitting. Due to different vaporization

157   schemes between the HR-AMS and SP-AMS, mass spectra from these two instruments

158   even for the same population of aerosols are not entirely the same. Because laser-only

159   SP-AMS generally results in less overall fragmentation, its mass profile may contain

160   more large *m/z* fragments and less small *m/z* fragments compared to that from HR-

161   AMS(Massoli et al., 2015). In addition, the elemental ratios of organics reported here,

162   i.e., oxygen-to-carbon and hydrogen-to-carbon ratios (O/C and H/C) were calculated

163   based on the "Improved-Ambient (I-A)" method(Canagaratna et al., 2015a) (scaling

164   factors of 1.10 for H:C and 0.86 for O:C were applied for elemental ratios calculated

165   from SP-AMS data)

166   Positive matrix factorization (PMF)(Paatero and Tapper, 1994) was performed on

167   the high-resolution organic mass spectra matrix of both NR-PM$_1$ and BC-PM$_1$ (e.g., BC

168   (C_x^+), and species associated with BC) across m/z 12–120 using PMF Evaluation Tool

169   written in Igor (Ulbrich et al., 2009), following the standard procedure (Zhang et al.,

170   2011). Four types of organic aerosol (OA) from total NR-PM$_1$ (see our previous

171   paper)(Xu et al., 2019b) and five OA factors from BC-PM$_1$ were identified. C_x^+ was

172   involved in the calculation of elemental ratios (e.g, O/C and H/C) of PMF OA factors.

173 All data presented in this paper were averaged hourly and are presented at local time

174 (Beijing Time, UTC+8).

175

176 **3. Results and discussion**

177 **3.1. Overview of observations**

178   Figure 1 shows the temporal variations of selected chemical species during the

179 campaign. Information for other variables is provided in the supplementary materials

180 (SM). The two cases labeled in Figure 1 are of interest. Case I (June 8-13) was

181 characterized with high NO_2 concentrations (average 26.7 ± 13.5 ppb, Table S1) and

182 relatively low O_3 concentrations (41.7 ± 30.0 ppb) with NO_2-to-O_3 ratio of 0.64. Case

183 II (June 17-22) was featured by low NO_2 (14.9 ± 5.9 ppb) and high O_3 (84.6 ± 30.6 ppb)

184 concentrations with an NO_2-to-O_3 ratio of 0.18. Unlike winter Beijing haze pollution,

185 *RH* remained at a relatively low level ($36.5 \pm 15.3\%$), which is not expected to play a

186 significant role in OA formation during the campaign (Figure 1b and Figure S1). In

187 contrast, a strong correlation has been observed between temperature and O_3 ($r^2 = 0.53$).

188 The temperature was higher on average in Case II (29.8 ± 3.8 ºC) than in Case I (26.1

189 ± 4.1 ºC).

190   The mass concentrations and mass concentration ratios of organic (Org), sulfate

191 (SO_4^{2-}) and nitrate (NO_3^-) in NR-PM_1 (in solid line) and BC-PM_1 (in dotted line) are

192 shown in Figures 1c-e. High correlations were observed between BC-PM_1 and NR-PM_1

193 measurements for SO_4^{2-} ($r^2 = 0.70$) and NO_3^- ($r^2 = 0.86$), but not for Org ($r^2 = 0.49$).

194 This result suggests that, BC-PM_1 Org has distinct sources or formation pathways from

195 NR-PM_1 Org. Comparing two cases, the average mass ratios of BC-PM_1 to NR-PM_1 for

196 SO_4^{2-} and NO_3^- in Case I (0.24 ± 0.11 and 0.37 ± 0.12) were close to those in Case II

197 (0.19 ± 0.06 and 0.31 ± 0.07). However, ratios of BC-PM_1 to NR-PM_1 for Org were a

198 factor of greater for Case I (0.74 ± 0.32) compare to Case II (0.46 ± 0.13). During the

199 nighttime, this ratio increases to almost unity in Case I. Additionally, BC concentration

200 in Case I (average 2.6 ± 1.6 µg m^{-3}) was 1.5 folds higher than in Case II (average $1.7 \pm$

201 0.8µg m^{-3}). The implication is that the organic is mostly associated with BC and likely

202 comprised of freshly emitted compounds in Case I. This is also evident by the moderate

203   correlation between NO_2 and BC-PM$_1$ Org ($r^2 = 0.42$) in Case I. On the other hand, the

204   lower Org ratio in Case II with higher O_3 concentrations indicates greater oxidation and

205   secondary processes in non-BC particles.

206

207   **3.2. Source apportionment of BC-PM$_1$ OA**

208   To further investigate the differences between organics in NR-PM$_1$ and BC-PM$_1$,

209   the comparison of PMF OA factors between NR-PM$_1$ and BC-PM$_1$ Org is necessary.

210   Four factors were identified from PMF analysis of the NR-PM$_1$ Org matrix, including

211   hydrocarbon-related OA (HOA), cooking OA (COA), less-oxidized oxygenated OA

212   (LO-OOA), and more-oxidized oxygenated OA (MO-OOA). Details of the NR-PM$_1$

213   PMF analysis can be found in our previous study (Xu et al., 2019b). Here we only

214   present the PMF results of the SP-AMS measured BC-PM$_1$ Org. As shown in Figure 2,

215   five factors were resolved by PMF with factors including a HOA, a less oxidized OOA

216   (OOA1), three more-oxidized OOA factors were recombined into one OOA factor

217   (MO-OOA= Aged- biomass burning organic aerosol (A-BBOA) + OOA2 + OOA3).

218   Diagnostic plots of this PMF solution is presented in Figure S2.

219   HOA consists of a series of hydrocarbon fragments ($C_xH_y^+$) in its mass spectrum

220   (Figure 2f), thus having a low O/C ratio (0.13) but a high H/C ratio (1.62). It has a r^2 of

221   0.92 with $C_4H_9^+$ (m/z = 57) and a r^2 of 0.57 with NO_x (Figure 2a), indicative of its

222   sources from vehicle emissions (Xu et al., 2019a). It also correlated tightly with BC (r^2

223   of 0.70) and a series of polycyclic aromatic hydrocarbons (PAHs) ions, e.g., $C_9H_7^+$ (m/z

224   115, r^2 of 0.63).

225   The second factor has a remarkably high fraction of the biomass burning organic

226   aerosol (BBOA) marker ions of $C_2H_4O_2^+$ (m/z = 60) (1.31%) and $C_3H_5O_2^+$ (m/z = 73)

227   (1.34%) in its mass spectrum (Figure 2g), much higher than that observed in non-BBOA

228   (e.g., 0.3% at m/z = 60) in previous studies (Sun et al., 2016;Xu et al., 2019a;Wang et

229   al., 2017). As expected, the temporal variation of this factor correlated tightly with those

230   of $C_2H_4O_2^+$ and $C_3H_5O_2^+$ (r^2 of 0.71 and 0.72, respectively). In addition, the mass

231   spectrum of this factor is strikingly similar to that of the transported BBOA which was

232   observed at a remote site in the central Tibetan Plateau (Wang et al., 2017), with a r^2 of

233   0.97. Here we categorized the transported BBOA as aged-BBOA (A-BBOA) identified

234   in this study. Similar to the A-BBOA observed in Tibetan Plateau, which has an O/C

235   ratio of 0.51, this factor also has a relatively high O/C ratio of 0.48, greater than that of

236   primary BBOA (O/C of 0.18−0.26)(Wang et al., 2017). These findings support that the

237   second factor may be associated with the oxidation of biomass burning emissions. The

238   temporal variation of ABBOA in the Tibetan Plateau was reported to be highly

239   correlated with the potassium ion fraction (K^+, r^2 of 0.78), and $K_3SO_4^+$ (r^2 of 0.92).

240   However, the temporal variation of the second factor in this study is only correlated

241   well with that of $K_3SO_4^+$ (r^2 of 0.64) but not K^+ (r^2 of 0.01). The reason for this

242   phenomenon is that the major source of K^+ in remote sites like the Tibetan Plateau was

243   long-distance transport of K_2SO_4 particles, which probably from biomass burning-

244   related K-containing salts interacts with H_2SO_4 (Buxton et al., 1999). In contrast, there

245   are multiple primary sources of K^+ in PM_1 (e.g., diesel-vehicle emissions, and mainly

246   KCl particles) in urban areas (Figure S3). Based on these observations, $K_3SO_4^+$ could

247   be defined as an external A-BBOA indicator. Moreover, a previous transmission

248   electron microscopy study also showed that significant agricultural BBOA was mixed

249   with soot and transport from the North China Plain to urban Beijing, meanwhile, K_2SO_4

250   was also identified within those single BBOA-soot particles (Li et al., 2010). Hence,

251   this second factor is identified as A-BBOA that was subjected to oxidation during

252   transport to the measurement area as presented in the fire-point map and three-day back

253   trajectories (Figure S4). June should be the month with maximum agricultural-related

254   biomass burning in the North China Plain, although we thought that such burning

255   activities had been banned in recent years (Shen et al., 2019).

256   The OOA1 factor has an O/C of 0.28 (Figure 2h). Similar to the NR-PM_1 LO-OOA

257   (Xu et al., 2019b), it is highly correlated with $C_2H_3O^+$ (r^2 of 0.72). The $C_2H_3O^+$ ion (m/z

258   = 43) is an important component of secondary organic aerosol (SOA)(Collier et al.,

259   2015;Ng et al., 2011) and the diurnal patterns of the OOA1 and $C_2H_3O^+$ both show a

260   great enhancement around noontime (Figure S5), indicating the importance of

261   secondary formation of less oxidized organic aerosol through daytime photochemical

262   activity.

263   The OOA2 factor has an O/C of 0.42 (Figure 2i) and the OOA3 factor has a smaller

264   O/C of 0.32 (Figure 2j). OOA2 correlated strongly with sulfate (r^2 of 0.92; Figure 2d)

265   and OOA3 correlated highly with nitrate (r^2 of 0.97; Figure 2e). These features agree

266   well with the previous observation for low-volatility OOA (sulfate-related OOA) and

267   semi-volatile OOA (nitrate-related OOA) in Tibetan Plateau (Wang et al., 2017).

3.3. Comparison of NR-PM$_1$ and BC-PM$_1$ OA factors

The sum of the above-mentioned BC-PM$_1$ A-BBOA, OOA2, and OOA3 fractions is comparable to the NR-PM$_1$ MO-OOA factor, based on their high O/C ratios. Figures 3a-c are comparisons of the mass loadings of HOA, LO-OOA, and MO-OOA in both NR-PM$_1$ and BC-PM$_1$. NR-PM$_1$ HOA, LO-OOA, and MO-OOA are strongly correlated with their counterpart fractions of BC-PM$_1$, with r^2 values of 0.68, 0.60, and 0.61, respectively. In Case I, most of the time, the mass loadings of BC-PM$_1$ HOA and MO-OOA are higher than those in NR-PM$_1$, while LO-OOA shows the opposite trend. In Case II, the mass loadings of BC-PM$_1$ HOA are also generally higher than those of NR-PM$_1$ HOA, however, NR-PM$_1$ MO-OOA and LO-OOA are almost two folds higher than those of BC-PM$_1$. Figures 3d-f are comparisons of the fractions of HOA, LO-OOA, and MO-OOA in NR-PM$_1$ and non-BC material in BC-PM$_1$ (coatings), respectively. In Case I, the fractions of HOA and MO-OOA internally-mixed with BC are almost two times and four times higher, respectively, than those in NR-PM$_1$, whereas the two LO-OOA fractions closely track each other. In Case II, two LO-OOA fractions are still overlapped, but compared to Case I, the fraction of HOA in BC-PM$_1$ coatings is over four times that of NR-PM$_1$ HOA, and the difference between the two MO-OOA fractions is smaller.

As shown in Figure 4, the average of BC-PM$_1$ HOA fractions (0.27 ± 0.17 and 0.11 ± 0.07, respectively) are higher than those in NR-PM$_1$ (0.12 ± 0.08 and 0.02 ± 0.02, respectively) in both Case I and Case II, indicating that HOA particles is more internally mixed with BC compared to other OA materials. However, the possibility that RIE of OA coating may be lower than the default RIE value should also be considered.

The average mass loadings of NR-PM$_1$ LO-OOA in both Case I and Case II were higher than those of BC-PM$_1$. However, the fraction of LO-OOA in both NR-PM$_1$ and BC-PM$_1$ coatings were very close to each other during the two cases, with an average value of 0.23 ± 0.10 and 0.25 ± 0.12, respectively, indicating that the probability of LO-OOA condensation onto the two different types of particles is similar.

A greater difference between the MO-OOA fractions in NR-PM$_1$ and BC-PM$_1$ was observed in Case I than in Case II, and there is more MO-OOA in BC-PM$_1$ than in NR-PM$_1$ in Case I. A similar comparison between NR-PM$_1$ MO-OOA with BC-PM$_1$ MO-

298   OOA without A-BBOA can be found in SI (Figure S6), which shows closer fractions in

299   both Case I and Case II. Therefore, one possibility that may cause higher MO-OOA

300   fraction in BC-PM$_1$ than that in NR-PM$_1$ in Case I is the presence of the BC-PM$_1$ A-

301   BBOA, which is only identified from the BC-PM$_1$ OA. More details of the BC-PM$_1$ A-

302   BBOA are discussed in Section 3.4.

303

304   3.4. Characteristics of A-BBOA in BC-containing PM$_1$

305   Figure 5 shows the high-resolution mass spectra of A-BBOA observed in Nam Co

306   (June 2015) and Beijing (June 2017) by laser-only SP-AMS. A mass spectra very

307   similar to that observed in Beijing was also observed in Nanjing (February 2017)(Wu

308   et al., 2019), with a r^2 of 0.95. The A-BBOA observed in Nam Co (the Tibetan Plateau)

309   was found in the thickest coated and internally-mixed BC-PM$_1$ (the mass ratio of

310   coatings to BC core (R_{BC}) can reach 14), which enhances the light absorption ability

311   (E_{abs}) of the BC core by a factor of 1.5 to 2.0 via the "lensing effect".

312   As shown in Figure 6, A-BBOA was associated with those large particles ($D_{va} >$

313   300nm) which were also heavily-coated ($R_{BC} > 9$, Figure 6a and 6c). Because A-BBOA

314   is a moderately aged OA, the OSc was very steady when $R_{BC} > 9$ (Figure 6c). Figure

315   6b presents the fractions of the OA factors (left) and the degree of light absorption

316   enhancement (E_{abs}, estimated by the mass ratios of BC measured by Aethalometer

317   model 33 and SP-AMS), as a function of R_{BC}. Figure 6d shows the temporal variations

318   of the fractions of NR-PM$_1$ OA and BC-PM$_1$ OA from 15:00 to 24:00 on June 17, 2017

319   when the highest A-BBOA concentrations were observed. There is a significant

320   enhancement of A-BBOA which may account for up to 60% of the total OA coatings,

321   which could enhance the BC-PM$_1$ MO-OOA fraction (within the purple frame in the

322   bottom panel of Figure 6d).

323   In this study, A-BBOA was only observed by SP-AMS and was indeed only

324   associated with BC. It is likely that A-BBOA was emitted together with BC when

325   burning biomass fuel, and was oxidized subsequently during the transport. However,

326   we cannot exclude the possibility that A-BBOA can be detected by HR-AMS. For

327   example, it might be included in NR-PM$_1$ MO-OOA factor. Without separating A-

328   BBOA from other organic species, the source apportionment for HR-AMS may obscure

329   air-quality- and climate-related implications of A-BBOA in the atmosphere, such as the

330   enhancement of aerosol light absorption ability (Figure 6b).

4. Conclusions and implications

Online chemical characteristics of BC and its associated species was for the first time elucidated in urban Beijing in summer, and compared with those of NR-PM$_1$ species. The biggest difference between the two measurements was in the composition of the organic species. In particular, we found BC in urban Beijing in June is partially of agricultural fire origin and, an unique biomass burning-related OA factor (A-BBOA) which was moderately aged, only existed in thickly coated BC-PM$_1$ ($R_{BC} > 9$), but not NR-PM$_1$. The unique A-BBOA could make up a significant portion of BC coating material. In addition to Beijing, similar A-BBOA was also identified in other locations, such as central Tibet Plateau (Wang et al., 2017) and Nanjing (Wu et al., 2019), suggesting that it may be ubiquitously present in BC-PM$_1$ in ambient atmosphere.

BBOA species are known to constitute a large portion of light-absorbing organics (brown carbon, BrC). The delay of BBOA oxidation and its longer duration time on BC cores can extend the impacts of BC. Moreover, together with our previous study of BC-associated A-BBOA in Tibet, results presented herein demonstrate that A-BBOA could lead to thick coating on BC cores, meaning a significant "lensing effect" to the enhancement of BC light absorption (Liu et al., 2017). As a key component of BC coating, presence of this factor may also alter the bulk hygroscopicity of BC-PM$_1$. It could therefore affect its ability as cloud condensation nuclei (CCN)(Wu et al., 2019). Overall, the emission, evolution and transport of such A-BBOA, may influence the atmospheric behaviors and influence the role of BC in the air quality and climate (e.g., radiative forcing and precipitation). We propose that future laboratory, field, and modeling studies are needed to verify the presence of A-BBOA, and to evaluate the regional environmental impacts of it.

Code/data availability. The data in this study are available from the authors upon request (caxinra@163.com or wangjunfeng@seas.harvard.edu).

Supplement. The supplement related to this article is available online at: xxx.

Author contributions. JF, DL, YW, JZ, WX, CX, FS and XG conducted the measurements and analyzed the data. JF, JY and PO wrote the first draft, JZ, PO, YQ, XZ, AL, SM, PF, DJ, QZ, YS, MC and XG contributed to the analyses and improvement of the paper. JF and XG contributed to the revision of the paper.

Competing interests. The authors declare that they have no conflict of interest.

Special issue statement. This article is part of the special issue "In-depth study of air pollution sources and processes within Beijing and its surrounding region (APHH-Beijing) (ACP/AMT inter-journal SI)". It is not associated with a conference.

Acknowledgements. The authors from PRC acknowledge support from the National Natural Science Foundation of China (21777073) and the National Key Research and Development Program of China (No. 2018YFC0213802). The authors from Harvard and NUIST acknowledge additional support through the Harvard-NUIST Joint Laboratory for Air Quality and Climate (JLAQC).

Financial support. This work was supported by the National Natural Science Foundation of China (21777073), National Key Research and Development Program of China (No. 2018YFC0213802), and the Harvard-NUIST Joint Laboratory for Air Quality and Climate (JLAQC).

ABBREVIATIONS

BC Black carbon

PM_1 Particulate matter with an aerodynamic diameter smaller than 1 μm

NR-PM_1 non-refractory PM_1

BC-PM_1 BC-containing particles in PM_1

BrC Brown carbon

HR-AMS High-resolution aerosol mass spectrometer (Aerodyne Research Inc.)

SP-AMS Soot-particle aerosol mass spectrometer (Aerodyne Research Inc.)

IE Ionization efficiency

RIE Relative ionization efficiency

HRMS High-resolution mass spectra

PMF Positive matrix factorization

OA Organic aerosol

SOA Secondary organic aerosolO/C Oxygen-to-carbon ratio

H/C Hydrogen-to-carbon ratio

A-BBOA Aged biomass burning organic aerosol

SV-OOA Semi-volatile oxygenated organic aerosol

LV-OOA low-volatility oxygenated organic aerosol

MO-OOA more-oxidized oxygenated organic aerosol

LO-OOA less-oxidized oxygenated organic aerosol

R_{BC} mass ratio of BC coatings to BC

D_{va} Vacuum aerodynamic diameter

References

356 Bond, T. C., Doherty, S. J., Fahey, D. W., Forster, P. M., Berntsen, T., DeAngelo, B. J., Flanner, M.
357 G., Ghan, S., Kärcher, B., Koch, D., Kinne, S., Kondo, Y., Quinn, P. K., Sarofim, M. C., Schultz, M.
358 G., Schulz, M., Venkataraman, C., Zhang, H., Zhang, S., Bellouin, N., Guttikunda, S. K., Hopke, P.
359 K., Jacobson, M. Z., Kaiser, J. W., Klimont, Z., Lohmann, U., Schwarz, J. P., Shindell, D., Storelvmo,
360 T., Warren, S. G., and Zender, C. S.: Bounding the role of black carbon in the climate system: A
361 scientific assessment, J. Geophys. Res.- Atmos, 118, 5380-5552, 10.1002/jgrd.50171, 2013.
362 Buseck, P. R., Adachi, K., Gelencsér, A., Tompa, É., and Pósfai, M.: Ns-Soot: A Material-Based
363 Term for Strongly Light-Absorbing Carbonaceous Particles, Aerosol Sci. Technol., 48, 777-788,
364 10.1080/02786826.2014.919374, 2014.
365 Canagaratna, M. R., Jayne, J. T., Jimenez, J. L., Allan, J. D., Alfarra, M. R., Zhang, Q., Onasch, T.
366 B., Drewnick, F., Coe, H., Middlebrook, A., Delia, A., Williams, L. R., Trimborn, A. M., Northway,
367 M. J., DeCarlo, P. F., Kolb, C. E., Davidovits, P., and Worsnop, D. R.: Chemical and microphysical
368 characterization of ambient aerosols with the aerodyne aerosol mass spectrometer, Mass Spectrom.
369 Rev., 26, 185-222, 10.1002/Mas.20115, 2007.
370 Canagaratna, M. R., Jimenez, J. L., Kroll, J. H., Chen, Q., Kessler, S. H., Massoli, P., Hildebrandt
371 Ruiz, L., Fortner, E., Williams, L. R., Wilson, K. R., Surratt, J. D., Donahue, N. M., Jayne, J. T., and
372 Worsnop, D. R.: Elemental ratio measurements of organic compounds using aerosol mass
373 spectrometry: characterization, improved calibration, and implications, Atmos. Chem. Phys., 15,
374 253-272, 10.5194/acp-15-253-2015, 2015a.
375 Canagaratna, M. R., Massoli, P., Browne, E. C., Franklin, J. P., Wilson, K. R., Onasch, T. B.,
376 Kirchstetter, T. W., Fortner, E. C., Kolb, C. E., Jayne, J. T., Kroll, J. H., and Worsnop, D. R.:
377 Chemical Compositions of Black Carbon Particle Cores and Coatings via Soot Particle Aerosol
378 Mass Spectrometry with Photoionization and Electron Ionization, J. Phys. Chem. A, 119, 4589-4599,
379 10.1021/jp510711u, 2015b.
380 Cappa, C. D., Onasch, T. B., Massoli, P., Worsnop, D. R., Bates, T. S., Cross, E. S., Davidovits, P.,
381 Hakala, J., Hayden, K. L., Jobson, B. T., Kolesar, K. R., Lack, D. A., Lerner, B. M., Li, S.-M.,
382 Mellon, D., Nuaaman, I., Olfert, J. S., Petäjä, T., Quinn, P. K., Song, C., Subramanian, R., Williams,
383 E. J., and Zaveri, R. A.: Radiative absorption enhancements due to the mixing state of atmospheric
384 black carbon, Science, 337, 1078-1081, 10.1126/science.1223447, 2012.
385 Chen, B., Andersson, A., Lee, M., Kirillova, E. N., Xiao, Q., Kruså, M., Shi, M., Hu, K., Lu, Z.,
386 Streets, D. G., Du, K., and Gustafsson, Ö.: Source Forensics of Black Carbon Aerosols from China,
387 Environ. Sci. Technol., 47, 9102-9108, 10.1021/es401599r, 2013.
388 Chen, Y.; Cai, J.; Wang, Z.; Peng, C.; Yao, X.; Tian, M.; Han, Y.; Shi, G.; Shi, Z.; Liu, Y.; Yang, X.;
389 Zheng, M.; Zhu, T.; He, K.; Zhang, Q.; Yang, F. Simultaneous measurements of urban and rural
390 particles in Beijing – Part 1: Chemical composition and mixing state. Atmos. Chem. Phys., 20, 9231-
391 9247, 10.5194/acp-20-9231-2020, 2020a.
392 Chen, Y.; Shi, G.; Cai, J.; Shi, Z.; Wang, Z.; Yao, X.; Tian, M.; Peng, C.; Han, Y.; Zhu, T.; Liu, Y.;
393 Yang, X.; Zheng, M.; Yang, F.; Zhang, Q.; He, K. Simultaneous measurements of urban and rural
394 particles in Beijing – Part 2: Case studies of haze events and regional transport. Atmos. Chem. Phys.,
395 20, 9249-9263, 10.5194/acp-20-9249-2020, 2020b.
396 China, S., Scarnato, B., Owen, R. C., Zhang, B., Ampadu, M. T., Kumar, S., Dzepina, K., Dziobak,
397 M. P., Fialho, P., Perlinger, J. A., Hueber, J., Helmig, D., Mazzoleni, L. R., and Mazzoleni, C.:
398 Morphology and mixing state of aged soot particles at a remote marine free troposphere site:

399   Implications for optical properties, Geophys. Res. Lett., 42, 1243-1250, 10.1002/2014gl062404,
400   2015.

401   Collier, S., Zhou, S., Kuwayama, T., Forestieri, S., Brady, J., Zhang, M., Kleeman, M., Cappa, C.,
402   Bertram, T., and Zhang, Q.: Organic PM Emissions from Vehicles: Composition, O/C Ratio, and
403   Dependence on PM Concentration, Aerosol Sci. Technol., 49, 86-97,
404   10.1080/02786826.2014.1003364, 2015.

405   Ge, X., Zhang, Q., Sun, Y., Ruehl, C. R., and Setyan, A.: Effect of aqueous-phase processing on
406   aerosol chemistry and size distributions in Fresno, California, during wintertime, Environ. Chem.,
407   9, 221-235, http://dx.doi.org/10.1071/EN11168, 2012a.

408   Ge, X. L., Setyan, A., Sun, Y., and Zhang, Q.: Primary and secondary organic aerosols in Fresno,
409   California during wintertime: Results from high resolution aerosol mass spectrometry, J. Geophys.
410   Res.- Atmos., 117, D19301, 10.1029/2012jd018026, 2012b.

411   Janssen, N.A.H., Gerlofs-Nijland, M., Lanki, T., Salonen, R.O., Cassee, F., Hoek, G., Fischer, P.,
412   Brunekreef, B., Krzyzanowski, M, Health effects of black carbon, WHO, 2012.
413   https://www.euro.who.int/__data/assets/pdf_file/0004/162535/e96541.pdf?ua=1

414   Lee, A. K. Y., Chen, C. L., Liu, J., Price, D. J., Betha, R., Russell, L. M., Zhang, X., and Cappa, C.
415   D.: Formation of secondary organic aerosol coating on black carbon particles near vehicular
416   emissions, Atmos. Chem. Phys., 17, 15055-15067, 10.5194/acp-17-15055-2017, 2017.

417   Lee, B. P., Li, Y. J., Yu, J. Z., Louie, P. K. K., and Chan, C. K.: Physical and chemical
418   characterization of ambient aerosol by HR-ToF-AMS at a suburban site in Hong Kong during
419   springtime 2011, Journal of Geophysical Research: Atmospheres, n/a-n/a, 10.1002/jgrd.50658, 2013.

420   Li, W. J., Shao, L. Y., and Buseck, P. R.: Haze types in Beijing and the influence of agricultural
421   biomass burning, Atmos. Chem. Phys., 10, 8119-8130, 10.5194/acp-10-8119-2010, 2010.

422   Li, Y. J., Lee, B. P., Su, L., Fung, J. C. H., and Chan, C. K.: Seasonal characteristics of fine
423   particulate matter (PM) based on high-resolution time-of-flight aerosol mass spectrometric (HR-
424   ToF-AMS) measurements at the HKUST Supersite in Hong Kong, Atmos. Chem. Phys., 15, 37-53,
425   10.5194/acp-15-37-2015, 2015.

426   Liu, C., Chung, C. E., Yin, Y., and Schnaiter, M.: The absorption Ångström exponent of black carbon:
427   from numerical aspects, Atmos. Chem. Phys., 18, 6259-6273, 10.5194/acp-18-6259-2018, 2018.

428   Liu, D., Whitehead, J., Alfarra, M. R., Reyes-Villegas, E., Spracklen, Dominick V., Reddington,
429   Carly L., Kong, S., Williams, Paul I., Ting, Y.-C., Haslett, S., Taylor, Jonathan W., Flynn, Michael J.,
430   Morgan, William T., McFiggans, G., Coe, H., and Allan, James D.: Black-carbon absorption
431   enhancement in the atmosphere determined by particle mixing state, Nature Geosci., 10, 184-188,
432   10.1038/ngeo2901, 2017.

433   Liu, D., Joshi, R., Wang, J., Yu, C., Allan, J. D., Coe, H., Flynn, M. J., Xie, C., Lee, J., and Squires,
434   F.: Contrasting physical properties of black carbon in urban Beijing between winter and summer,
435   Atmos. Chem. Phys., 6749-6769, 2019.

436   Massoli, P., Onasch, T. B., Cappa, C. D., Nuamaan, I., Hakala, J., Hayden, K., Li, S.-M., Sueper, D.
437   T., Bates, T. S., Quinn, P. K., Jayne, J. T., and Worsnop, D. R.: Characterization of black carbon-
438   containing particles from soot particle aerosol mass spectrometer measurements on the R/V Atlantis
439   during CalNex 2010, J. Geophys. Res.- Atmos., 120, 2014JD022834, 2015.

440   Ng, N. L., Canagaratna, M. R., Jimenez, J. L., Chhabra, P. S., Seinfeld, J. H., and Worsnop, D. R.:
441   Changes in organic aerosol composition with aging inferred from aerosol mass spectra, Atmos.
442   Chem. Phys., 11, 6465-6474, 10.5194/acp-11-6465-2011, 2011.

Onasch, T. B., Trimborn, A., Fortner, E. C., Jayne, J. T., Kok, G. L., Williams, L. R., Davidovits, P., and Worsnop, D. R.: Soot Particle Aerosol Mass Spectrometer: Development, Validation, and Initial Application, Aerosol Science and Technology, 46, 804-817, 10.1080/02786826.2012.663948, 2012.

Paatero, P., and Tapper, U.: Positive matrix factorization: A non-negative factor model with optimal utilization of error estimates of data values, Environmetrics, 5, 111-126, 10.1002/env.3170050203, 1994.

Qiu, Y., Xie, Q., Wang, J., Xu, W., Li, L., Wang, Q., Zhao, J., Chen, Y., Chen, Y., Wu, Y., Du, W., Zhou, W., Lee, J., Zhao, C., Ge, X., Fu, P., Wang, Z., Worsnop, D. R., and Sun, Y.: Vertical Characterization and Source Apportionment of Water-Soluble Organic Aerosol with High-resolution Aerosol Mass Spectrometry in Beijing, China, ACS Earth Space Chem., 3, 273-284, 10.1021/acsearthspacechem.8b00155, 2019.

Ramanathan, V., and Carmichael, G.: Global and regional climate changes due to black carbon, Nature Geosci, 1, 221-227, 2008.

Saleh, R., Marks, M., Heo, J., Adams, P. J., Donahue, N. M., and Robinson, A. L.: Contribution of brown carbon and lensing to the direct radiative effect of carbonaceous aerosols from biomass and biofuel burning emissions, J. Geophys. Res.- Atmos., 120, 10,285-210,296, 10.1002/2015jd023697, 2015.

Shen, L., Jacob, D. J., Zhu, L., Zhang, Q., Zheng, B., Sulprizio, M. P., Li, K., De Smedt, I., González Abad, G., Cao, H., Fu, T.-M., and Liao, H.: The 2005–2016 Trends of Formaldehyde Columns Over China Observed by Satellites: Increasing Anthropogenic Emissions of Volatile Organic Compounds and Decreasing Agricultural Fire Emissions, Geophys. Res. Lett., 46, 4468-4475, 10.1029/2019gl082172, 2019.

Shi, Z., Vu, T., Kotthaus, S., Harrison, R. M., Grimmond, S., Yue, S., Zhu, T., Lee, J., Han, Y., Demuzere, M., Dunmore, R. E., Ren, L., Liu, D., Wang, Y., Wild, O., Allan, J., Acton, W. J., Barlow, J., Barratt, B., Beddows, D., Bloss, W. J., Calzolai, G., Carruthers, D., Carslaw, D. C., Chan, Q., Chatzidiakou, L., Chen, Y., Crilley, L., Coe, H., Dai, T., Doherty, R., Duan, F., Fu, P., Ge, B., Ge, M., Guan, D., Hamilton, J. F., He, K., Heal, M., Heard, D., Hewitt, C. N., Hollaway, M., Hu, M., Ji, D., Jiang, X., Jones, R., Kalberer, M., Kelly, F. J., Kramer, L., Langford, B., Lin, C., Lewis, A. C., Li, J., Li, W., Liu, H., Liu, J., Loh, M., Lu, K., Lucarelli, F., Mann, G., McFiggans, G., Miller, M. R., Mills, G., Monk, P., Nemitz, E., O'Connor, F., Ouyang, B., Palmer, P. I., Percival, C., Popoola, O., Reeves, C., Rickard, A. R., Shao, L., Shi, G., Sprucklen, D., Stevenson, D., Sun, Y., Sun, Z., Tao, S., Tong, S., Wang, Q., Wang, W., Wang, X., Wang, X., Wang, Z., Wei, L., Whalley, L., Wu, X., Wu, Z., Xie, P., Yang, F., Zhang, Q., Zhang, Y., Zhang, Y., and Zheng, M.: Introduction to the special issue "In-depth study of air pollution sources and processes within Beijing and its surrounding region (APHH-Beijing)", Atmos. Chem. Phys., 19, 7519-7546, 10.5194/acp-19-7519-2019, 2019.

Sun, Y., Jiang, Q., Wang, Z., Fu, P., Li, J., Yang, T., and Yin, Y.: Investigation of the Sources and Evolution Processes of Severe Haze Pollution in Beijing in January 2013, J. Geophys. Res.- Atmos., 2014JD021641, 10.1002/2014JD021641, 2014.

Sun, Y., Jiang, Q., Xu, Y., Ma, Y., Zhang, Y., Liu, X., Li, W., Wang, F., Li, J., Wang, P., and Li, Z.: Aerosol characterization over the North China Plain: Haze life cycle and biomass burning impacts in summer, J. Geophys. Res.- Atmos., 121, 2508-2521, 10.1002/2015jd024261, 2016.

Sun, Y. L., Zhang, Q., Schwab, J. J., Chen, W. N., Bae, M. S., Hung, H. M., Lin, Y. C., Ng, N. L., Jayne, J., Massoli, P., Williams, L. R., and Demerjian, K. L.: Characterization of near-highway submicron aerosols in New York City with a high-resolution aerosol mass spectrometer, Atmos.

Chem. Phys., 12, 2215-2227, 10.5194/acp-12-2215-2012, 2012.

Ulbrich, I. M., Canagaratna, M. R., Zhang, Q., Worsnop, D. R., and Jimenez, J. L.: Interpretation of organic components from Positive Matrix Factorization of aerosol mass spectrometric data, Atmos. Chem. Phys., 9, 2891-2918, 10.5194/acp-9-2891-2009, 2009.

V. Buxton, G., Bydder, M., and Arthur Salmon, G.: The reactivity of chlorine atoms in aqueous solution. Part II.The equilibrium $SO_4^-+Cl^-Cl^{Nsbd}+SO_4^{2-}$, Phys. Chem. Chem. Phys., 1, 269-273, 10.1039/A807808D, 1999.

Wang, J., Onasch, T. B., Ge, X., Collier, S., Zhang, Q., Sun, Y., Yu, H., Chen, M., Prévôt, A. S., and Worsnop, D. R.: Observation of fullerene soot in eastern China, Environ. Sci. Technol. Lett., 3, 121-126, 10.1021/acs.estlett.6b00044, 2016.

Wang, J., Zhang, Q., Chen, M., Collier, S., Zhou, S., Ge, X., Xu, J., Shi, J., Xie, C., and Hu, J.: First chemical characterization of refractory black carbon aerosols and associated coatings over the Tibetan Plateau (4730 m asl), Environ. Sci. Technol., 51, 14072-14082, 10.1021/acs.est.7b03973, 2017.

Wang, J., Liu, D., Ge, X., Wu, Y., Shen, F., Chen, M., Zhao, J., Xie, C., Wang, Q., and Xu, W.: Characterization of black carbon-containing fine particles in Beijing during wintertime, Atmos. Chem. Phys., 19, 447-458, 10.5194/acp-19-447-2019, 2019.

Willis, M. D., Lee, A. K. Y., Onasch, T. B., Fortner, E. C., Williams, L. R., Lambe, A. T., Worsnop, D. R., and Abbatt, J. P. D.: Collection efficiency of the soot-particle aerosol mass spectrometer (SP-AMS) for internally mixed particulate black carbon, Atmos. Meas. Tech., 7, 4507-4516, 10.5194/amt-7-4507-2014, 2014.

Wu, Y., Liu, D., Wang, J., Shen, F., Chen, Y., Cui, S., Ge, S., Wu, Y., Chen, M., and Ge, X.: Characterization of Size-Resolved Hygroscopicity of Black Carbon-Containing Particle in Urban Environment, Environ. Sci. Technol., 53, 14212-14221, 10.1021/acs.est.9b05546, 2019.

Xie, C., Xu, W., Wang, J., Liu, D., Ge, X., Zhang, Q., Wang, Q., Du, W., Zhao, J., Zhou, W., Li, J., Fu, P., Wang, Z., Worsnop, D., and Sun, Y.: Light absorption enhancement of black carbon in urban Beijing in summer, Atmos. Environ., 213, 499-504, 10.1016/j.atmosenv.2019.06.041, 2019a.

Xie, C., Xu, W., Wang, J., Wang, Q., Liu, D., Tang, G., Chen, P., Du, W., Zhao, J., and Zhang, Y.: Vertical characterization of aerosol optical properties and brown carbon in winter in urban Beijing, China, Atmos. Chem. Phys., 19, 165-179, 10.5194/acp-19-165-2019, 2019b.

Xu, J., Zhang, Q., Shi, J., Ge, X., Xie, C., Wang, J., Kang, S., Zhang, R., and Wang, Y.: Chemical characteristics of submicron particles at the central Tibetan Plateau: insights from aerosol mass spectrometry, Atmos. Chem. Phys., 18, 427-443, 10.5194/acp-18-427-2018, 2018.

Xu, W., Sun, Y., Wang, Q., Zhao, J., Wang, J., Ge, X., Xie, C., Zhou, W., Du, W., and Li, J.: Changes in aerosol chemistry from 2014 to 2016 in winter in Beijing: Insights from high-resolution aerosol mass spectrometry, J. Geophys. Res.- Atmos., 124, 1132-1147, 10.1029/2018JD029245, 2019a.

Xu, W., Xie, C., Karnezi, E., Zhang, Q., Wang, J., Pandis, S. N., Ge, X., Zhang, J., An, J., and Wang, Q.: Summertime aerosol volatility measurements in Beijing, China, Atmos Chem Phys, 19, 10205-10216, 10.5194/acp-19-10205-2019, 2019b.

Zhang, Q., Jimenez, J., Canagaratna, M., Ulbrich, I., Ng, N., Worsnop, D., and Sun, Y.: Understanding atmospheric organic aerosols via factor analysis of aerosol mass spectrometry: a review, Anal. Bioanal. Chem., 401, 3045-3067, 10.1007/s00216-011-5355-y, 2011.

529

530
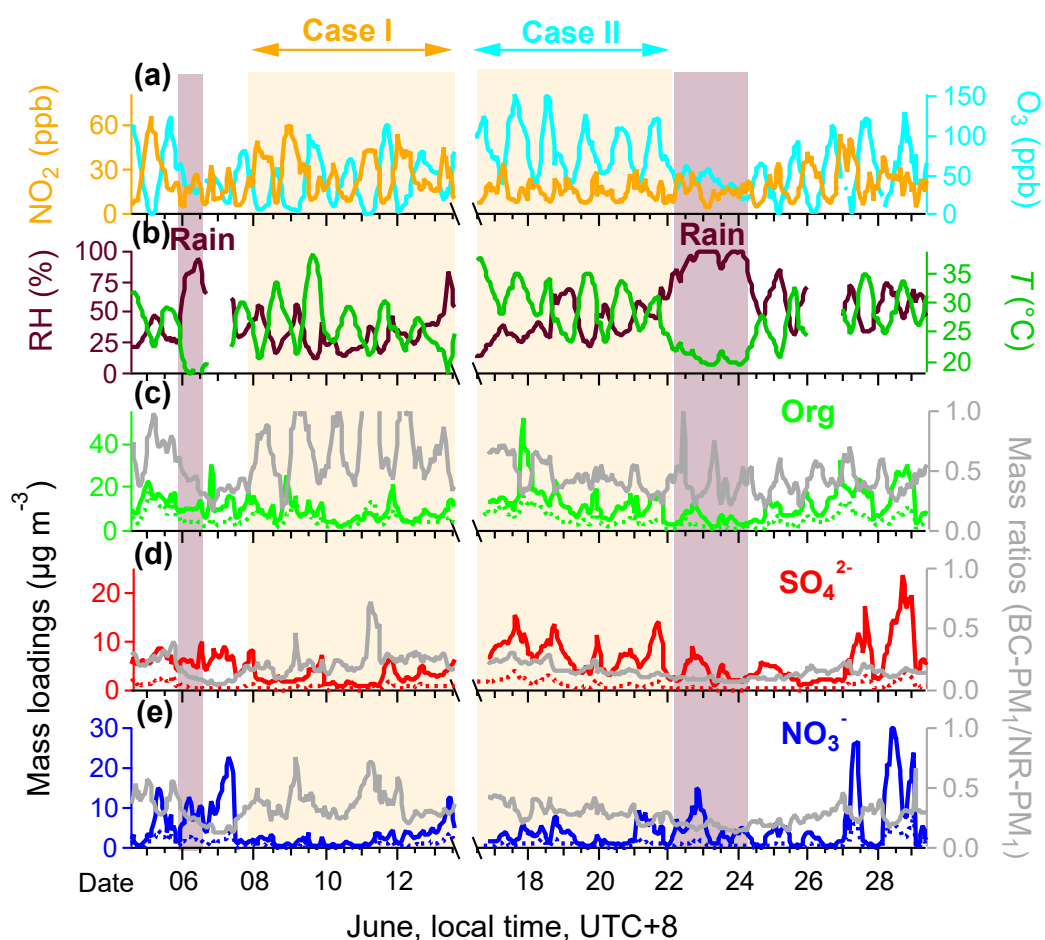
Figure 1. Temporal variations of selected chemical species measured in Beijing on June 4 -29, 2017. (a) mixing ratios of nitrogen dioxide (NO_2) and ozone (O_3); (b) 15-m relative humidity (*RH*) and temperature (*T*); (c-e) on the left are the mass loadings of organic (Org), sulfate (SO_4^{2-}) and nitrate (NO_3^-) measured by HR-AMS and SP-AMS, and on the right are mass ratios of individual BC-PM$_1$ species to NR-PM$_1$ species (e.g., BC-PM$_1$ Org to NR-PM$_1$ Org). The NR-PM$_1$ species measured by HR-AMS is in solid line, and the BC-PM$_1$ species measured by SP-AMS is in the dotted line. The shaded areas are raining periods. The observation period is divided into two cases according to the mixing ratio of nitrogen NO_2, Case I and Case II, which represent high NO_2 and low NO_2 mixing ratios, respectively.
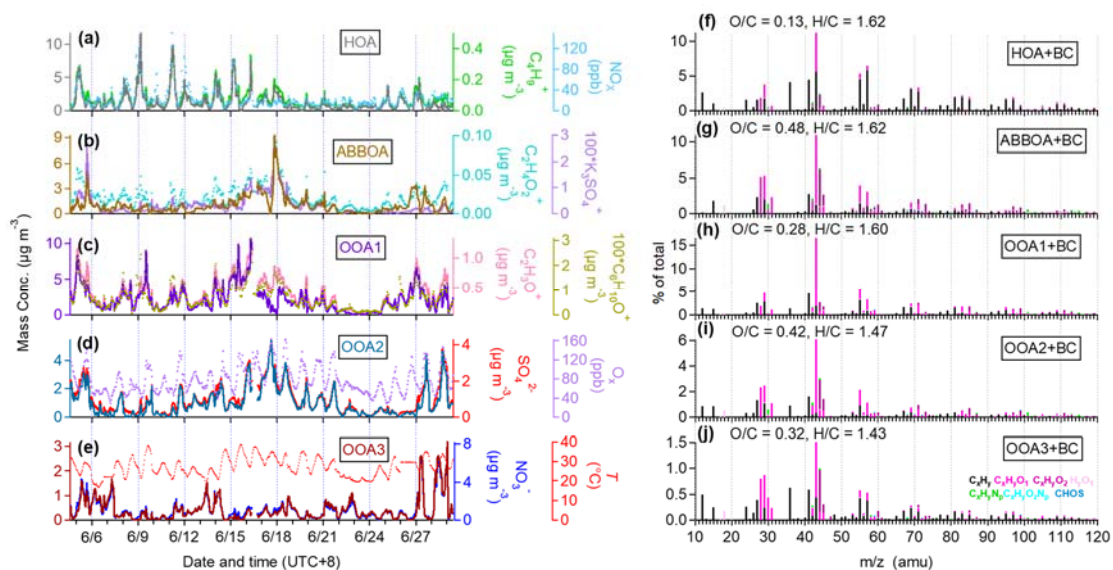
540

541 **Figure 2.** Temporal variations (left panels), high-resolution mass spectra (right panels) of five OA

542 factors in summer 2017: (a) and (f) HOA, (b) and (g) A-BBOA, (c) and (h) OOA1 (LO-OOA), (d)

543 and (i) OOA2, and (e) and (j) OOA3. Also shown in the left panels are the time series of other

544 tracers, including $C_4H_9^+$, NOx, $C_2H_4O_2^+$, $K_3SO_4^+$, $C_6H_{10}O^+$, $C_2H_3O^+$, SO_4^{2-} and NO_3^-.

545
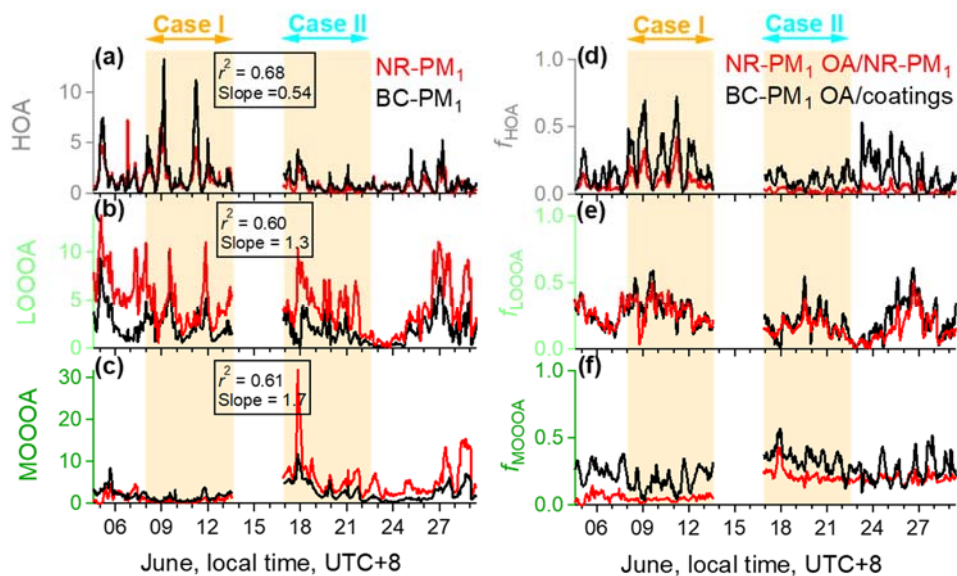
Figure 3. Temporal variations of NR-PM$_1$ and BC-PM$_1$ (a-c) HOA, LO-OOA, and MO-OOA (left panels) and (d-e) their fractions. NR-PM$_1$ OA factors are in red, and the BC-PM$_1$ OA factors are in black. Here BC-PM$_1$ MO-OOA is the sum of A-BBOA, OOA2 (sulfate-related OOA), and OOA3 (nitrate-related OOA).
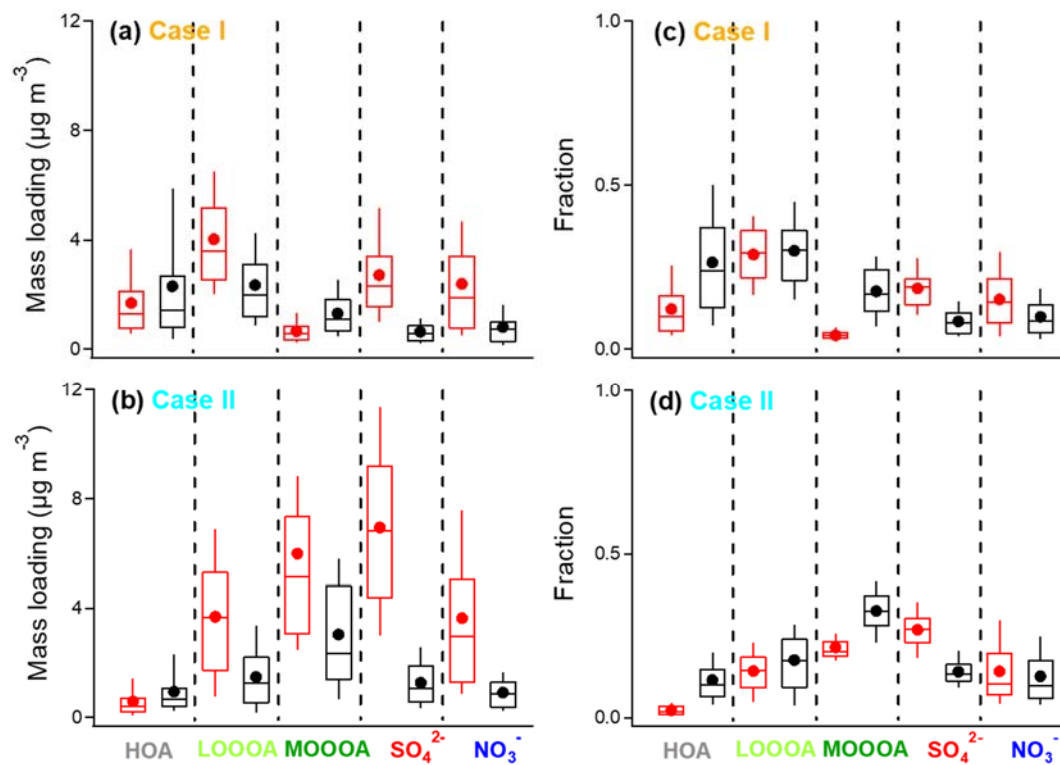
550

551   **Figure 4.** Box plots of mass loadings and fractions of five selected species (HOA, LO-OOA, MO-

552   OOA, SO_4^{2-}, and NO_3^-) in Case I and Case II. The bounds of boxes represent quartiles, the whiskers

553   indicate the 90th and 10th percentiles, and the lines and dots inside the boxes are median and mean

554   values. NR-PM_1 OA factors are in red, and the BC-PM_1 OA factors are in black.

555
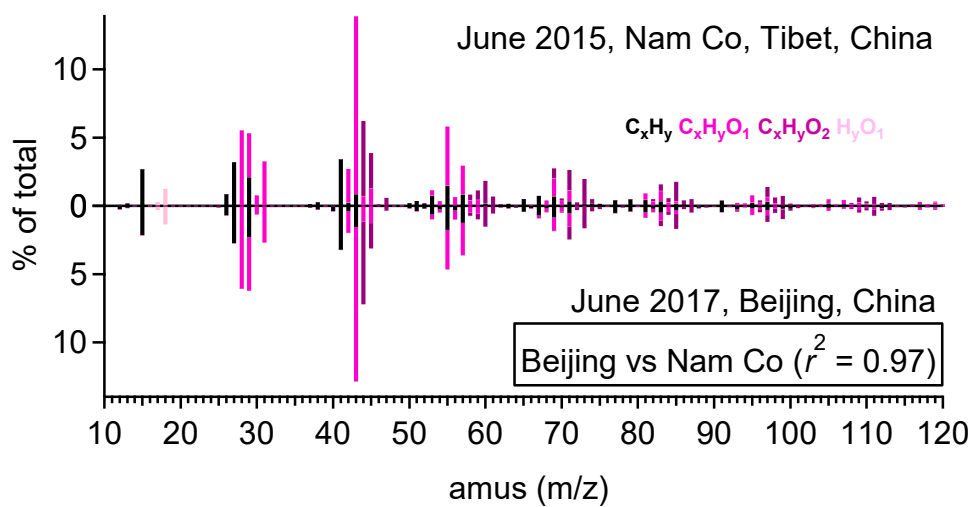
Figure 5 Comparison between the high-resolution mass spectra of A-BBOA obtained in Nam Co

556

(June 2015) and Beijing (June 2017) (nitrogen-containing ions are not shown here).

557
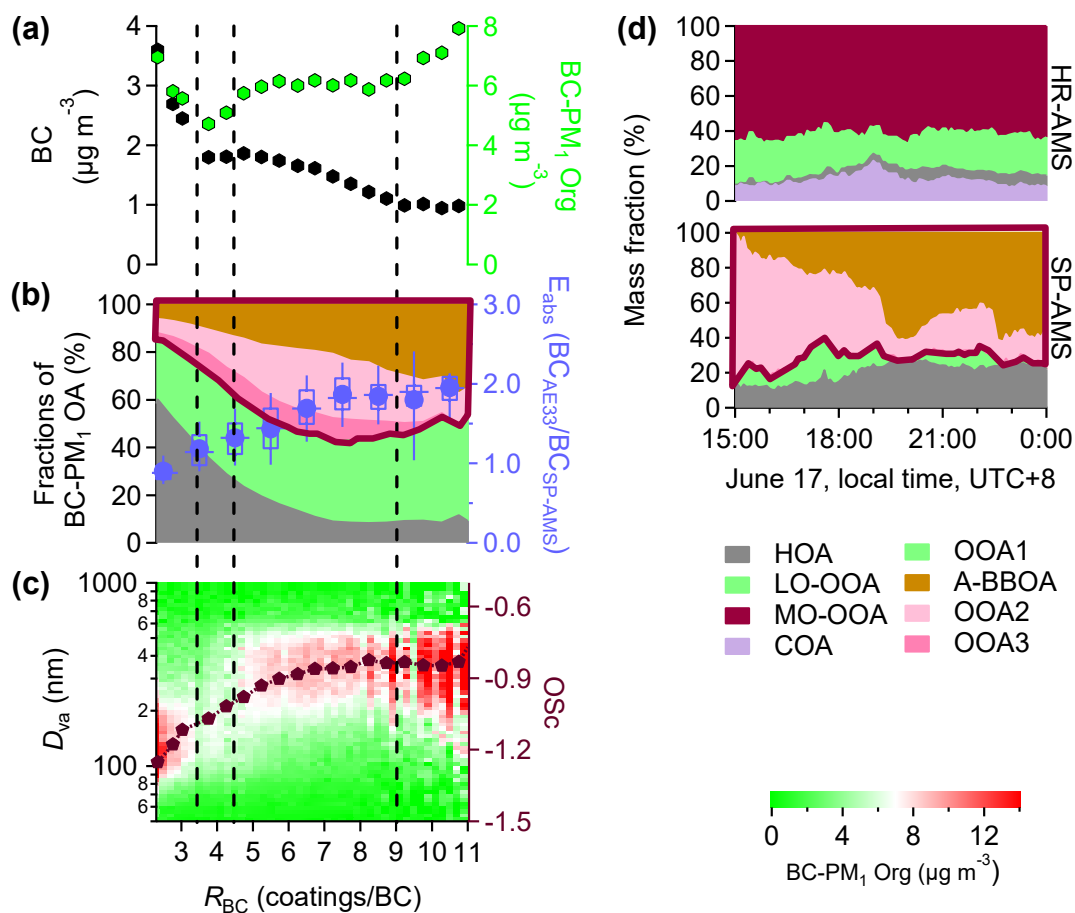
558

559 **Figure 6.** (a-c) the mass loadings of BC, BC-PM$_1$ Org, fractions of BC-PM$_1$ OA factors, E_{abs}, the

560 oxidation state (OSc = 2*(O/C) – (H/C)) of BC-PM$_1$ Org, and the size distribution of BC-PM$_1$ Org

561 as a function of coating thickness (R_{BC}). (d) temporal variations of OA fractions of NR-PM$_1$ and

562 BC-PM$_1$ from 15:00 to 24:00 on June 17, 2017.

563

564